INSTITUTE OF PHYSICS PUBLISHING PLASMA PHYSICS AND CONTROLLED FUSION

Plasma Phys. Control. Fusion **45** (2003) 233–250 PII: S0741-3335(03)54692-9

Role of the current density profile on drift wave stability in internal transport barrier reversed magnetic shear experiments at JET and Tore Supra

C Fourment, G T Hoang, L-G Eriksson, X Garbet, X Litaudon and G Tresset

EURATOM-CEA Association, CEA/DSM/DRFC, CEA Cadarache, 13108 St Paul-lez-Durance, France

Received 14 October 2002
Published 17 February 2003
Online at stacks.iop.org/PPCF/45/233

Abstract

The role of the current density profile on drift wave stability is investigated using a linear electrostatic gyro-kinetic code. The growth rates are shown to have a linear dependence on the normalized temperature gradients above a certain threshold. A parametric study of the threshold shows a dramatic stabilizing effect of negative magnetic shear, especially for large scale instabilities. A set of handy formulae fitting the threshold as a function of the magnetic shear and the safety factor is proposed. Analysis of reversed magnetic shear discharges with internal transport barrier (ITB) in JET shows that ion ITBs can be triggered by the negative magnetic shear in the core of the plasma. Subsequently, the increase of the $E \times B$ shearing rate allows for the expansion of the ITB, despite the increase of the linear growth rates due to the temperature gradient peaking. In the case of the electron ITB obtained in the Tore Supra LHEP mode, the central increase of the confinement is associated with the stabilization of large scale trapped electron modes by the negative magnetic shear effect, whereas the steep electron temperature gradient destabilizes the small scale electron temperature gradient modes, which prevent the electron heat transport to reach neoclassical levels.

1. Introduction

A tokamak plasma with an internal transport barrier (ITB) is a very attractive way to operate a commercially viable fusion reactor [1, 2]. An ITB can generally be defined as an internal region of the plasma where the energy transport is significantly reduced, possibly reaching the ion neoclassical level. In discharges exhibiting ITBs, the core energy confinement is improved leading to high fusion yields. Moreover, the pressure profiles in ITB plasma are often peaked, resulting in a large bootstrap fraction of the total plasma current, which would be beneficial for steady-state operation. It has been shown in several experiments that the access to such

an advanced regime is usually correlated with the reduction of the fluctuation associated with micro-instabilities [3–6].

The main physical mechanism of ITB formation is still not fully understood, and needs to be clarified. Several stabilizing mechanisms for micro-instabilities have been identified, namely: (i) magnetic shear effect in the precession drift of trapped particles and in the toroidal coupling of passing particles [7]; (ii) turbulence suppression by the shearing of the $E \times B$ rotation [6, 8, 9]; (iii) decrease of the radial correlation length for low magnetic shear [10, 11]; (iv) decrease of the radial correlation length or fluctuation amplitude due to nonlinear decorrelation of linearly unstable modes [12]; (iv) decrease of the destabilizing particles fraction when increasing the Shafranov shift parameter α ($\alpha = -q^2 R \partial\beta/\partial r$, R being the plasma major radius, r the minor radius and β the normalized kinetic pressure to the magnetic pressure) [7, 13]. The analysis of experiments show that the ITB formation can be attributed to different characteristics of the plasma: sheared poloidal flow, due to a gradient of the radial electric field [14, 15] or a MHD mode coupling between a flux surface where the safety factor is rational and the edge of the plasma [16]; low or reversed magnetic shear [17, 18]; Shafranov shift [13].

Since the first pellet enhanced performance (PEP) mode observed in JET [19], current profile control experiments, allowing one to obtain a reversed magnetic shear configuration have been intensively investigated in many devices. Such experiments have provided very promising results [20–22].

In this work, we try to clarify the physics underlying the ITBs in the reversed magnetic shear experiments performed at JET and Tore Supra. For this purpose, we used a linear gyro-kinetic code, KINEZERO [23, 24], to identify the key parameters for triggering and sustaining ITBs by stabilizing the electrostatic microinstabilities. In the two next sections, we study the parametric dependence of the micro-instabilities upon the magnetic shear s, the safety factor q and the parameter α: in section 2, the linear growth rates are addressed and the section 3 is devoted to the dependence of the normalized critical temperature gradient length ($(R/L_\mathrm{T})_\mathrm{c} = R/(T/\nabla T)_\mathrm{c}$, R being the plasma major radius). An empirical formula of the critical threshold is also proposed. Ion ITBs observed in JET experiments are analysed in section 4. In section 5, an electron ITB case in Tore Supra is addressed. Finally, a summary is drawn in section 6.

2. Linear growth rates

Linear growth rates calculation is the natural way to investigate the conditions for the existence of turbulence and to identify the key parameters yielding to a stabilization as we plan to do. In our work, the linear growth rates are computed with a linear gyro-kinetic code, KINEZERO [23, 24]. The maximum growth rate, $\gamma^{\max}$, of the unstable electrostatic eigenmodes is calculated for 16 radial positions. For a given radial position, the spectrum of γ covers 40 values of the toroidal wavenumber (n). In the current version of the code, the Shafranov shift effect is implemented with displaced circular magnetic flux surfaces [25]. In addition, for each unstable mode the driving power P_l transferred from the particles to the mode is evaluated from the imaginary part of the complex product $\omega \cdot L_l$.

$$P_l = \mathrm{Im}(\omega \cdot L_l) \tag{1}$$

Here, the index l denotes the particle species (trapped ions, trapped electrons, passing ions or passing electrons); ω is the complex pulsation of the mode (real part is the frequency and imaginary part is the growth rate); and L_l is the non adiabatic response of the particles l. This quantity contains useful information for identifying which type of particle is responsible

for the turbulence. Indeed, if the particles l globally destabilize the modes, P_l is positive. Otherwise, P_l is negative. In the KINEZERO code, a complete toroidal spectrum is calculated by taking into account the non-adiabatic response of both ion and electron populations. It covers large scale ($k_\perp \rho_\mathrm{i} < 1$, where ρ_i is the ion Larmor radius and $k_\perp$ is the wave vector in the direction perpendicular to the magnetic field) and small scale ($k_\perp \rho_\mathrm{i} > 1$) instabilities. In this study, we separate the $\gamma^{\max}$ toroidal spectrum into two parts. The first part of the spectrum, $k_\perp \rho_\mathrm{i} < 1$, corresponds to trapped ion and ion temperature gradient (ITG) modes and the upper wave-length spectrum of the trapped electron mode (TEM). In the second part, $k_\perp \rho_\mathrm{i} > 1$, the ion response is assumed to be adiabatic due to the spatial average during the cyclotron motion, thus the instabilities can be attributed to the lower wave-length spectrum of TEM and the electron temperature gradient (ETG) modes. In the following, we will call $\gamma^{\max}_{\mathrm{ITG+TEM}}$ the maximum growth rate in the first part of the spectrum, and $\gamma^{\max}_{\mathrm{ETG}}$ the maximum growth rate in the second one.

In these calculations, the current profile is parametrized via 3 parameters: s, q and α. Typical variations of $\gamma^{\max}$, at mid-radius, with s, q and α separately are illustrated in figures 1(a)–(c). The plasma parameters in figure 1 were: $R = 3\,\mathrm{m}$, $a = 0.9\,\mathrm{m}$, toroidal magnetic field $B = 2\,\mathrm{T}$, $n_\mathrm{e} = 4 \times 10^{19}\,\mathrm{m}^{-3}$, $T_\mathrm{e} = T_\mathrm{i} = 3\,\mathrm{keV}$, $R/L_\mathrm{n} = 0$ ($L_\mathrm{n} = n/\nabla n$), $R/L_\mathrm{T} = 14$ in figure 1(a), $R/L_\mathrm{T} = 10$ in figures 1(b) and (c), $Z_\mathrm{eff} = 1$. The parameters s, q and α when not being varied were fixed at 1, 2, and 0, respectively. In figure 1(a), we can see that the maximum growth rate of ITG, TEM and ETG modes, decreases roughly linearly with the absolute value of s. Furthermore, negative values are more efficient in reducing $\gamma^{\max}$. These trends are qualitatively in agreement with the results of a two-dimensional global gyro-kinetic simulation [26]. Note that owing to the first order ballooning transform used

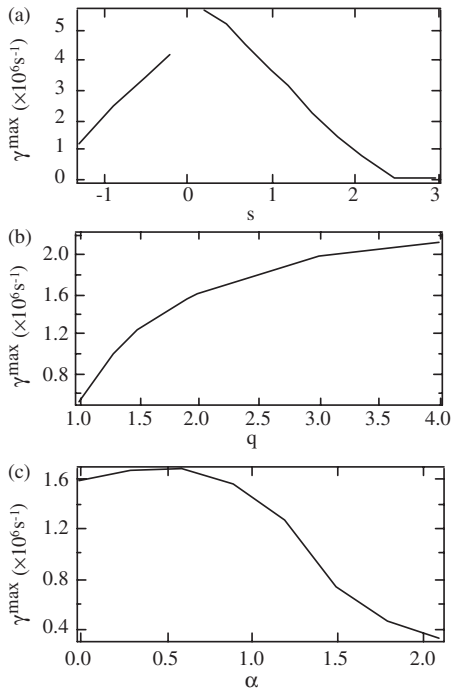

Figure 1. Maximum linear growth rate versus magnetic shear (a), safety factor (b) and α parameter (c).

in KINEZERO, the zone around $s = 0$ is not accessible in our calculations. Figure 1(b) indicates that increasing q increases $\gamma^{\max}$, and this destabilizing effect seems to saturate for q values above 3. The Shafranov shift effect is displayed in figure 1(c). This figure suggests the existence of a threshold above which $\gamma^{\max}$ significantly decreases: $\alpha \approx 1$ for the set of parameters used in our calculation. No α dependence in $\gamma^{\max}$ is observed below this threshold.

3. Critical temperature gradient length

The variation of the linear growth rates as discussed in the previous section are direct indicators of the possible stabilization by the s, q and α parameters. However, for convenience it is more valuable to deal with the plasma temperature gradient lengths instead of the linear growth rates, as the temperature gradient length is more directly evaluated from experimental measurements. The existence of a critical temperature gradient length below which micro turbulence develops is predicted by many anomalous transport models based on either analytical stability theory or numerical simulations [27–35]. Strong evidence for such a critical threshold has been provided by electron transport analyses of experimental data [36, 37] and also from measurements of both density [38] and magnetic fluctuations [39].

In this work, we calculate the linear growth rates ($\gamma^{\max}$) for various values of R/L_{T}, keeping the other parameters constant. $\gamma^{\max}$ is found to vary linearly with R/L_{T} as depicted in figure 2, and can be parametrized as:

$$\gamma^{\max} = R_\gamma \left[\frac{R}{L_{\mathrm{T}}} - \left(\frac{R}{L_{\mathrm{T}}} \right)_{\mathrm{c}} \right] \tag{2}$$

The critical threshold $(R/L_{\mathrm{T}})_{\mathrm{c}}$ is determined as a finite value of R/L_{T} for which $\gamma^{\max}$ vanishes, using a linear extrapolation. The parameter R_γ determines the stiffness of $\gamma^{\max}$ versus R/L_{T}. Both $(R/L_{\mathrm{T}})_{\mathrm{c}}$ and R_γ are the functions of the local plasma parameters ($s, q, T, n, \ldots$). A sheared slab ITG model, proposed by Hahm and Tang [32], predicts a s/q dependence

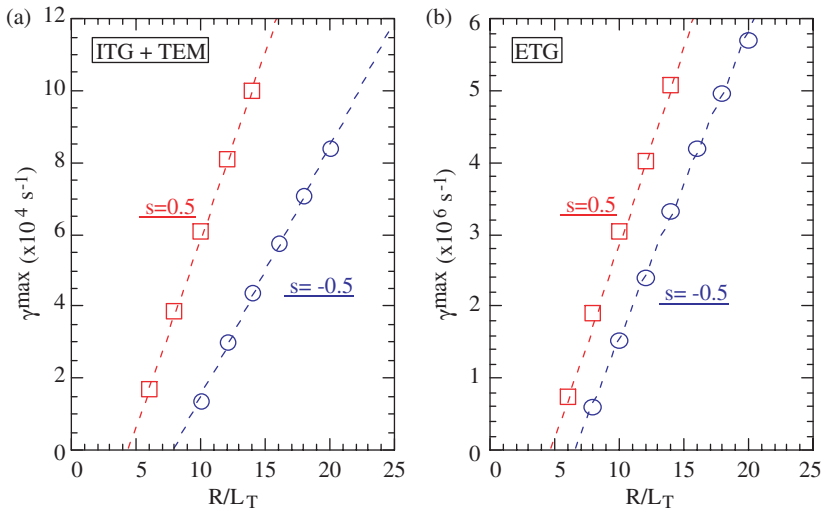

Figure 2. Linear growth rate versus temperature gradient length for ITG + TEM (a) and ETG (b) modes.

in $(R/L_{T_i})_c$:

$$\left(\frac{R}{L_{T_i}}\right)_c = 1.88\frac{s}{q}\left(1+\frac{T_i}{T_e}\right) \tag{3}$$

Experimentally, the Tore Supra discharges, in which the electrons were dominantly heated by the fast waves, suggested an empirical offset linear expression for $(R/L_{T_e})_c$ [40]

$$\left(\frac{R}{L_{T_e}}\right)_c = 5+10\frac{s}{q} \tag{4}$$

for $s > 0$ and $(Z_{eff}T_e/T_i)$ almost constant. This is consistent with a recent computation for the ETG modes which also provided an offset term, due to the toroidal geometry [41]

$$\left(\frac{R}{L_{T_e}}\right)_c = \left(1.33+1.91\frac{s}{q}\right)\left(1+Z_{eff}\frac{T_e}{T_i}\right) \tag{5}$$

In the next paragraphs, the parametric dependence of both $(R/L_T)_c$ and R_γ upon s and q, at $\alpha = 0$, are studied. We used the same set of plasma parameters as mentioned in section 2. It is worth noting that for this data set, the most unstable ITG + TEM modes propagate in the ion diamagnetic direction ('ITG-like'). Thus, the linear growth rates of the ITG + TEM modes mentioned in the following are denoted as $\gamma^{max}_{ITG\text{-}like}$.

3.1. Magnetic shear dependence of $(R/L_T)_c$

To study the magnetic shear dependence in $(R/L_T)_c$ we varied s between -1 and 3, keeping $q = 2$. $(R/L_T)_c$ is determined for the ETG and ITG-like modes, respectively. As shown in figure 3, $(R/L_T)_c$ varies almost linearly with s, in agreement with equations (3)–(5). The critical thresholds are not symmetric with respect to negative/positive s values. For the ITG-like branch, a negative value of s is clearly more stabilizing than a positive one, while it weakly affects the ETG branch. Moreover, the thresholds of ITG-like and ETG are very similar for $s > 0$, whereas for $s < 0$ the ITG-like modes are more stable than the ETG modes, resulting in higher values of $(R/L_T)_c$. This difference can be explained by evaluating P_l (equation (1)). Trapped electrons are found to be very sensitive to negative value of s for ITG-like. For the ETG modes, the trapped/passing electrons are destabilizing, and ions are adiabatic. In contrast, for the ITG-like modes, the trapped/passing ions are destabilizing, but the trapped electrons are stabilizing.

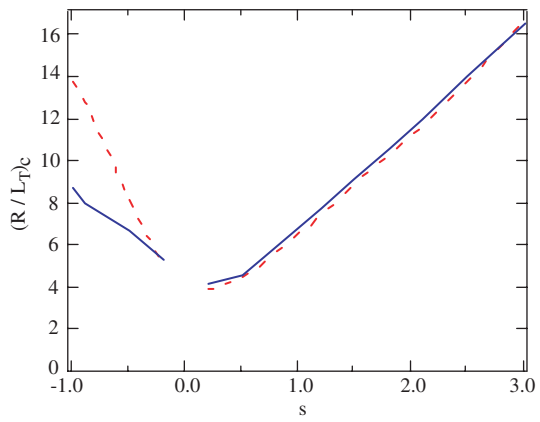

Figure 3. Variation of critical temperature gradient length with magnetic shear (——: ETG; - - - -: ITG + TEM, mostly ITG-like).

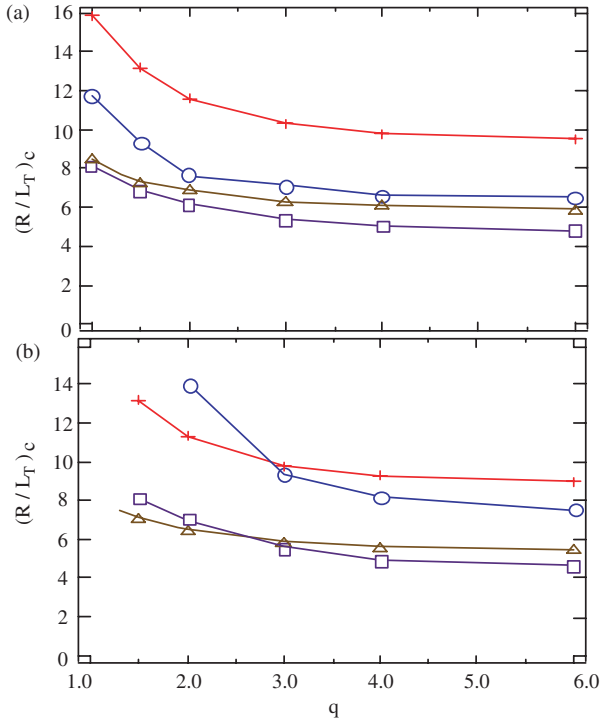

Figure 4. Variation of critical temperature gradient length with safety factor, for ETG (*a*) and ITG + TEM (*b*) modes. +: $s = 2$; ○: $s = -0.8$; △: $s = 1$; □: $s = -0.4$.

3.2. Safety factor dependence of $(R/L_T)_c$

A q dependence study has been done by varying q from 1 to 6, at fixed value of s ranging from -0.8 and 2. As shown in figure 4 $(R/L_T)_c$ decreases with increasing q, at each given s value, for both the ETG and ITG-like modes. For a q value above 2 $(R/L_T)_c$ seems to become independent of q, especially for $s > 1$ or $s < 0$. This trend is qualitatively in agreement with the results of simulations of the ETG threshold in [41]. Thus, these results can suggest that the q value has little influence on the critical threshold in the confinement region for high q-edge value experiments, in which the local q is usually higher than 2.

3.3. Stiffness in linear growth rates

As shown in figures 3 and 4, the critical thresholds of the ETG modes are close to the ITG-like value. On the contrary, the value of R_γ in equation (2), which determines the stiffness of $\gamma^{\max}$ versus R/L_T, is found to be quite different. It is stressed that the γ-stiffness is different than the stiffness of the turbulent diffusivity. Here, γ-stiffness describes the increase of the growth rates when the temperature gradient exceeds the critical threshold, but it does not give any indication on the correlation length and the diffusivity. The γ-stiffness for ETG modes is two orders of magnitude larger than that of ITG-like modes (figure 5). As a consequence, $\gamma^{\max}_{\text{ETG}}$ is much larger than $\gamma^{\max}_{\text{ITG-like}}$. This result indicates that the stabilization of ETG turbulence is more difficult than that of ITG-like. Variations of the γ-stiffness with s and q have been studied. For both the ITG-like and ETG modes, R_γ significantly decreases with an increasing absolute value of s (figure 5(*a*)). Thus, the magnetic shear plays a key role in the linear growth rates

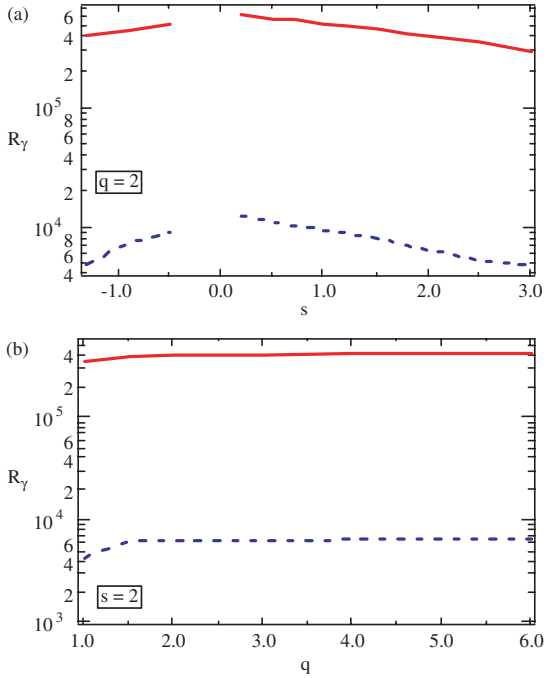

Figure 5. γ-stiffness (R_γ factor in equation (1)) versus magnetic shear (*a*) and safety factor (*b*) (——: ETG; - - - -: ITG + TEM).

Table 1. Empirical expressions of $2 \times (R/L_T)_c$.

$s > 0$	ETG and ITG-like	$1.1 + 1.4\|s\| + 1.9\|s\|/q$ (6)	$\sigma = 3\%$
$s < 0$	ETG	$2 + 0.4\|s\| + 4.2\|s\|/q$ (7)	$\sigma = 4\%$
$s < 0$	ITG-like	$0.9 + 1.6\|s\| + 9.9\|s\|/q$ (8)	$\sigma = 7\%$

through both the γ-stiffness and the critical gradient length. Conversely, the safety factor does not affect the γ-stiffness (figure 5(*b*)).

3.4. Empirical expression of critical temperature gradient length

A parameter scan has been carried out in the plane (s, q): $-1.3 < s < 3$ at $q = 2$; $1 < q < 6$ at $s = -0.8$, -0.4, 1 and 2, respectively. We only considered the case $\alpha = 0$, since the dependence of $(R/L_T)_c$ on α is rather complex (in particular, it interferes with s and q dependencies), and we fixed $T_e/T_i = 1$, $Z_{eff} = 1$, $R/L_n = 0$. According to the trends described above, the trial fitting functions have been generated by the basis $(1, s, 1/q)$. Best fits on this basis give the expressions of type: $(R/L_T)_c = C_1 + C_2 s + C_3 s/q$ (C_i being constant). The results for each type of instability are shown in table 1.

σ is defined as:

$$\sigma = \sqrt{\frac{\sum((R/L_T)_c^{fit} - (R/L_T)_c)^2}{\sum((R/L_T)_c)^2}}$$

Table 1 shows clearly a asymmetry with respect to $s = 0$, especially for the ITG-like modes. An offset linear dependence on the ratio s/q (i.e. $C_1 + C_2 s/q$) was also obtained, similar to the results in [32, 41]. But in this case, the fits are not as good as than equation (6)–(8) ($\sigma \approx 15\%$).

As mentioned above, $\gamma^{\max}$ is expected to vary weakly with α for $\alpha < 1$. Thus, the formulae in table 1 are valid for moderate values of α. When the α value becomes important, the equations (6)–(8) are no longer adequate. In addition, the phenomena involved in the ITG-like branch are very complex due to the interplay between the responses of trapped electrons and passing ions. The dependence of ITG-like critical threshold on the density peaking, assumed to be flat here, is therefore expected to be significant.

4. Stability analysis of ion ITBs in reversed magnetic shear discharges at JET

Recent JET experiments have been dedicated to the control of ITBs by optimizing the current profile by combining NBI with RF heating (ICRH and LHCD) [42, 43]. LHCD was used to preform an initially hollow current profile before the application of NBI and ICRH. In this section, we present a comprehensive analysis of drift wave stability in such plasmas at both the moment of the ion ITB onset and when the ITB is fully developed. At this point, we recall that KINEZERO uses an s-α model with very large aspect ratio and circular flux surfaces. In order to use KINEZERO in the cases of a shaped plasma, we are taking into account finite aspect ratio effects in a simplified way. Following the argument of [41]: for the toroidal modes in the ballooning approximation, the relevant radius in the normalized gradients is the local value of the major radius on the equatorial plane at the low-field side, $R = (1 + \varepsilon)R_0$, where R_0 is the major radius of the flux surface axis and $\varepsilon = r/R_0$. This was implemented in KINEZERO by taking as input the gradient lengths normalized by $(1 + \varepsilon)R_0$ instead of R_0. As far as the triangularity and the elongation of the plasma are concerned, a systematic study using the GS2 code shows that their effect is weak (less than 20%) on the linear critical gradient value of the toroidal ETG modes, and it is supposed to be of the same order for the ITG modes [41]. ITG linear gyro-kinetic comparison in a real and an s-α geometry have been performed by Waltz and Miller [44] using the GS2 code in the DIIID discharge #84736 test case. The authors found a variation of 20–30% on the linear growth rates, but no simple law accounting for the variation was observed. Thus, the circular geometry introduces some limitations, but the errors made are relatively modest. As a consequence, a rapid code such as KINZERO is still a very useful tool for studying the trends, i.e. parametric dependencies, of the linear growth rates. The effect of collisions is also neglected. This approximation is valid when the effective collision frequency is smaller than the vertical drift frequency of trapped electrons. Here, the plasma we analysed have low density (less than $5 \times 10^{19}\,\mathrm{m}^{-3}$) and temperatures ranging from 3 keV (pre-ITB phase) to 10 keV (ITB phase). In these regimes and particularly in the core of the discharge, the effective collision frequency (typically $4 \times 10^4\,\mathrm{s}^{-1}$) is 1–2 orders of magnitude smaller than the vertical drift frequency (about $10^6\,\mathrm{s}^{-1}$) for toroidal wave number such as $k_\perp r_\mathrm{i} = 1$, which supports the approximation we make in the KINEZERO code.

4.1. Role of the current profile for triggering ion ITBs

In this section, we carefully analyse the pre-ITB phase, i.e. the moment when the barrier is formed. A clear example showing the role of the current profile in the formation of ITBs for two JET discharges was analysed in [17]. It consists in comparing two JET discharges characterized by the same target parameters, but completely different q-profiles before an ITB is formed. As shown in figure 6, both discharges had $I_\mathrm{p} = 2.2\,\mathrm{MA}/B_\mathrm{T} = 2.6\,\mathrm{T}$; LHCD (2 MW) was applied very early during the current ramp-up phase in the first one (#51613) in order to create a non-monotonic q-profile (figure 7), and it was switched-off just before the NBI/ICRH (respectively 10 MW and 2 MW) application. The reversed shear discharge #51613 clearly displayed an ITBs in both the electron and ion channels at $t = 5.7$ s, during NBI and

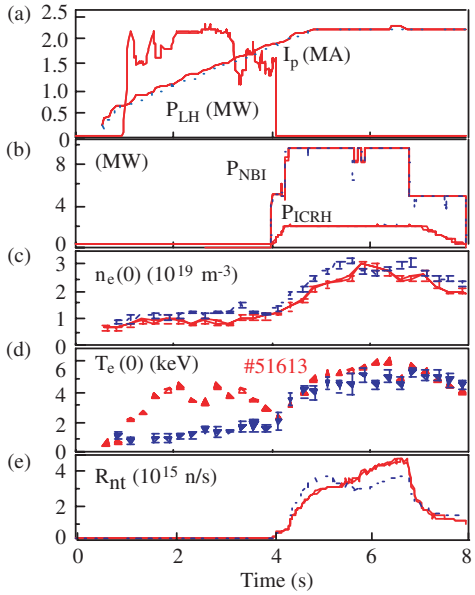

Figure 6. Comparison of two JET discharges: with (——, #51613) and without (- - - -, #51611) ITB: (*a*) plasma current and LH power; (*b*) neutral beam and ICRH powers; (*c*) central electron density; (*d*) central electron temperature; (*e*) neutron rate.

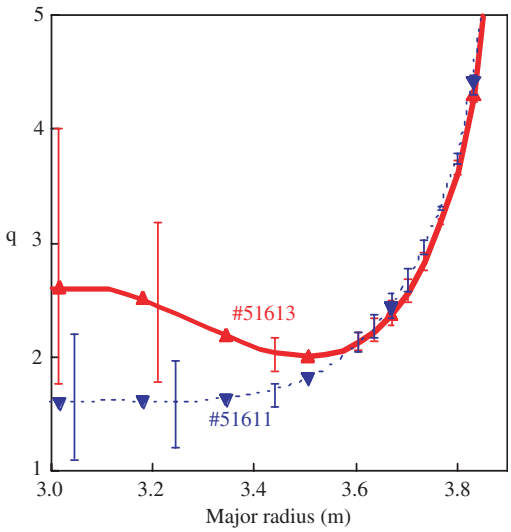

Figure 7. q-profiles measured at 5.7 s for both shots in figure 6 (——: #51613, - - - -: #51611).

ICRH applications (temperature profiles and neutron rate signals), which correspond to a wide zone of reduced transport. The barrier was localized roughly at normalized radius (defined as the squared root of the normalized toroidal flux) of 0.5. On the contrary, no transition was observed in the discharge with monotonic q-profile (#51611), although the same amount of NBI and ICRH powers was applied.

On of the prime candidates to that could have varied with the q-profile in the two discharges is, of course, the stability of the turbulent modes. We have investigated this possibility with the KINEZERO code. At the time $t = 5.7$ s, just before the ITB formation, both TEMs and ETGs were found to be stabilized for shot #51613, as shown in figure 8. Furthermore, the linear growth rate of the ITG-like branch, $\gamma^{\max}$ (as defined in section 2) was significantly different in the two discharges. Its radial profile, shown in figure 9(a), displays a strong reduction inside the barrier for #51613, whereas for shot #51611 $\gamma^{\max}$ stays high in most of the central region of the plasma. In order to assess the reliability of the conclusion that $\gamma^{\max}$ is reduced in a significantly larger region for #51613 than for #51611, we have calculated error bars, represented by the shaded regions in figure 9(a), by varying the temperature and density profiles within their respective error bars. As can be seen, the uncertainties are considerable. However, the error bar on the extent of the stabilized region for #51613 is less than 3 cm, and the point where $\gamma^{\max}$ becomes zero for #51611 is hardly changed at all. Furthermore, outside the error bars, $\gamma^{\max}$ is lower in the region inside normalized radius 0.4, i.e. almost the whole ITB region, for #51613 than for #51611. Thus, one can have some confidence in our conclusions regarding the differences in the stabilized regions between the two discharges.

The decrease of the core $\gamma^{\max}$ value in the discharge #51613 is clearly linked to the q-profile. Two candidates are likely to be responsible here: (i) negative magnetic shear; (ii) high q value in the reversed shear region, through the α parameter which depends on q^2. In order to identify the main parameter, we have evaluated the α effect by replacing the α value in #51613 by the value of shot #51611 without ITB transition. The corresponding $\gamma^{\max}$ indicates that the α-stabilization is almost negligible inside the barrier (figure 9(b)). This comparison strongly suggests that the negative s is a crucial factor for decreasing $\gamma^{\max}$ in the case of discharge #51613.

In analysing the causes of the barrier formation in #51613 we must also look at other factors that could have contributed. The results of non-linear simulations [43] suggests the

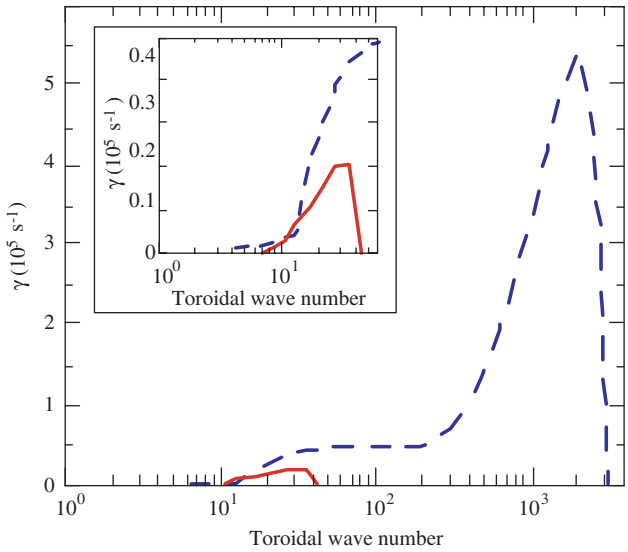

Figure 8. Linear growth rate spectra of discharges in figure 6, performed at $t = 5.7$ s, for $r/a = 0.45$.

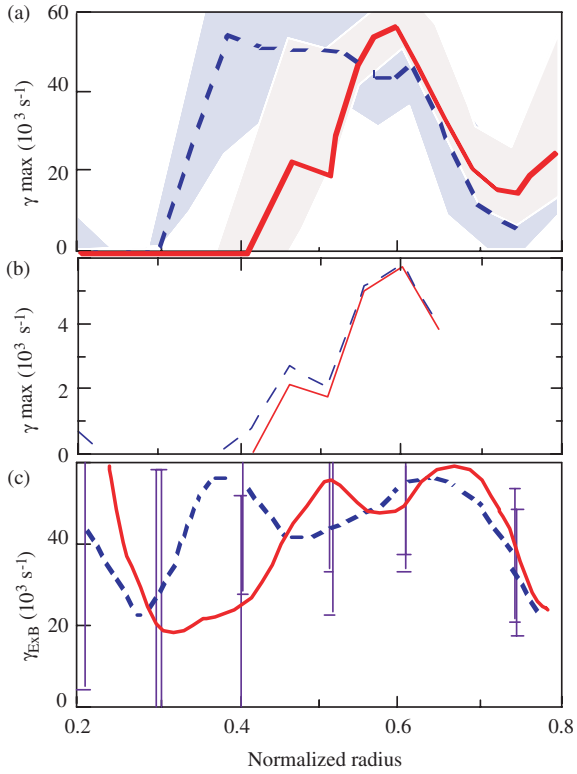

Figure 9. Radial profiles of $\gamma_{\rm lin}^{\rm max}(k_\perp \rho_{\rm i} < 1)$ and $\gamma_{E\times B}$ for both shots figure 6, performed at $t = 5.7$ s: (*a*) $\gamma_{\rm lin}^{\rm max}$ (——: #51613, - - - -: #51611). (*b*) $\gamma_{\rm lin}^{\rm max}$ for shot #51613 (- - - -: using α value of shot #51611). (*c*) $\gamma_{E\times B}$ (——: #51613, - - - -: #51611).

following condition for turbulence suppression:

$$\gamma_{E\times B} > k\gamma^{\rm max} \tag{9}$$

where k is a factor of order unity. Therefore, the ITBs can be triggered either by decreasing $\gamma^{\rm max}$ or by increasing the shearing rate $\gamma_{E\times B}$. Owing to the dependence of these two parameters on the current and pressure profiles, which are non-linearly coupled, it is generally difficult to identify the relative importance of the q-profile on them. However, for the two discharges discussed here, it is relatively clear that differences in $\gamma^{\rm max}$ cannot explain the wide barrier in shot #51613 (cf [16]). We have evaluated, $\gamma_{E\times B}$, from the Hahm–Burrell formula [44]:

$$\gamma_{E\times B} = \frac{RB_{\rm p}}{B}\frac{\partial}{\partial r}\left(\frac{E_r}{RB_{\rm p}}\right) \tag{10}$$

The radial electric field is derived from the equilibrium force balance equation [6] for the carbon impurity, using the measured carbon pressure and toroidal rotation.

$$E_r = \frac{\nabla P_{\rm c}}{Z_{\rm c} e n_{\rm c}} + B_{\rm p}V_{\varphi{\rm c}} - B_\varphi V_{\rm pc} \tag{11}$$

The poloidal rotation is calculated with a neoclassical formula [45]. The very marginal differences in radial profiles of $\gamma_{E\times B}$, within the error bars, shown in figure 9(*c*), cannot explain the wide barrier in shot #51613 (cf [16]). If anything, the shearing rate for #51611 is higher than for #51613. Thus, there are strong indications the decrease of $\gamma^{\rm max}$ due to negative s is an important factor in the barrier formation in discharge #51613.

4.2. Role of the $E \times B$ shearing for maintaining ion ITB

ITBs, sustained in quasi steady-state conditions by combining 15 MW of NBI, 4 MW of ICRH and 3 MW of LHCD, have been achieved in reversed magnetic shear configurations at JET [41]. The LH power was initially applied to form a hollow current profile and then to maintain such a profile during the high performance ITB phase. The time evolution of the ion temperature profile of discharge #53521 is reported in figure 10(*a*). Once again, the analyses of this discharge show the essential role of magnetic shear during the pre-ITB phase. First, $\gamma^{\max}$ drops, due to negative s, and becomes lower than $\gamma_{E\times B}$, as shown in figure 11, in which the radial profiles of $\gamma^{\max}$ and $\gamma_{E\times B}$ are calculated at three selected time slices just after the ITB triggering.

Then, once the ITB is fully formed, the effect of α in $\gamma^{\max}$ becomes significant. On the contrary with the pre-ITB phase, in which α is about 0.8, α reached a value of about 3 (figure 10(*b*)). Both the negative magnetic shear and the large α keep $\gamma^{\max}$ at low values in the strong temperature gradient region, in spite of the destabilizing effect of a strong temperature gradient during full ITB (figure 12). Furthermore there is a significant increase of the $E \times B$ shearing rate inside the barrier, allowing the ITB sustained in steady-state condition (satisfying the stabilization condition in equation (9)).

Note that the observed stabilizing influence of s and α are consistent with theory, which predicts the same fundamental mechanism for sufficiently negative s and high α: the reversal of the precession drift of the barely trapped particles and the decrease of the toroidal coupling of passing particles. In order to identify which particles are responsible for turbulence, we have evaluated the mean driving power transferred to the most unstable mode by each type of particle, P_l (in equation (1)), for shot #53521 (in figure 10) at $t = 8$ s. The results show that the trapped ions/electrons destabilize the modes. Whereas the passing ions are stabilizing and the passing electrons have an adiabatic behavior (figure 13(*a*)). For comparison, a computation

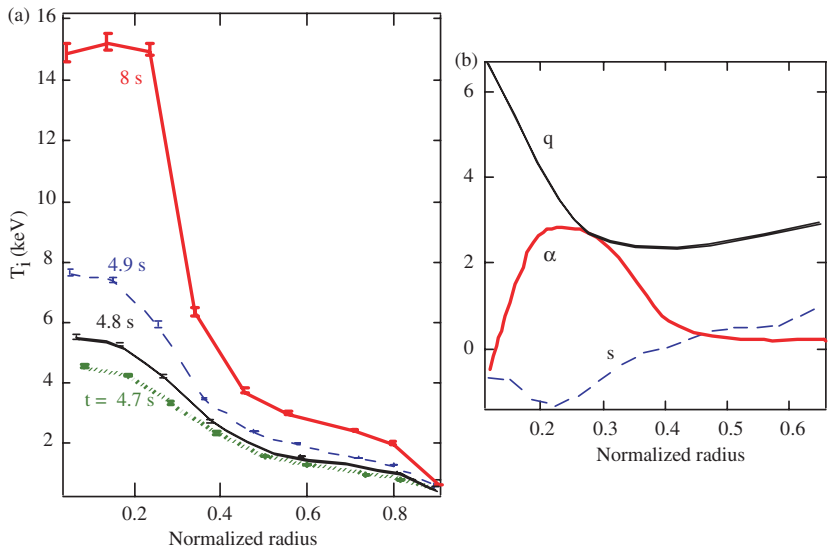

Figure 10. Ion ITB sustained in a quasi steady-state JET discharge (#53521) heated by combined NBI (15 MW), ICRH (4 MW) and LHCD (3 MW). (*a*) Ion temperature profiles at various times (ITB is formed at $t = 4.7$ s). (*b*) Radial profile of safety factor (q), magnetic shear (s) and Shafranov shift parameter (α) during the full development of the ion ITB ($t = 8$ s).

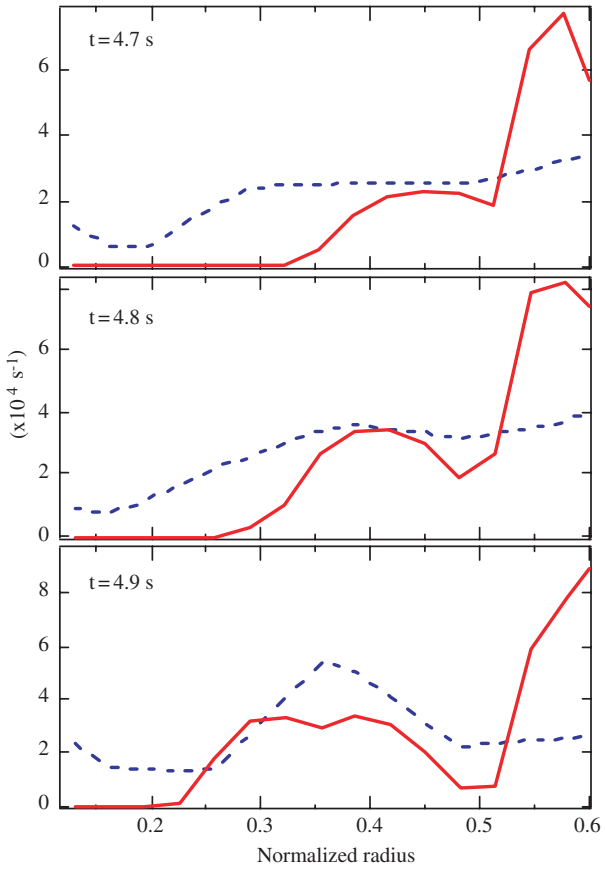

Figure 11. Radial profile of linear growth rate (——) compared with $E \times B$ shearing rate (- - - -) for discharge mentioned in figure 10.

assuming a monotonic q-profile has been performed (figure 13(b)). In this case, the passing ions/electrons destabilize the modes of low and very high wave number, respectively. Trapped electrons destabilize the modes rather in the medium wave number range. This yields a continuous spectrum with much higher growth rates than in the reversed current profile case, as shown in figure 14.

5. Stability analysis of the electron ITBs in reversed magnetic shear discharges at Tore Supra

This section deals with LHCD Tore Supra plasmas exhibiting an electron ITB. The experiments were carried out in helium, at $I_p = 0.7\,\mathrm{MA}$, $B_T = 3.9\,\mathrm{T}$ and central electron density $n_e(0) = 2.5 \times 10^{19}\,\mathrm{m}^{-3}$ [17]. Only the electron ITB transition was observed because the LH power was mostly coupled to the electrons and the ion–electron equipartition was weak. A typical discharge (#28334, so-called LHEP, i.e. lower hybrid enhanced performance) is shown in figure 15. An LH power of 4 MW was applied at 6 s on the current flat top. At $t = 7.2\,\mathrm{s}$, the electron ITB transition was observed inside the region $r/a \leqslant 0.3$, together with a non-monotonic q-profile (figure 15(b)). The electron ITB is characterized by an increase of

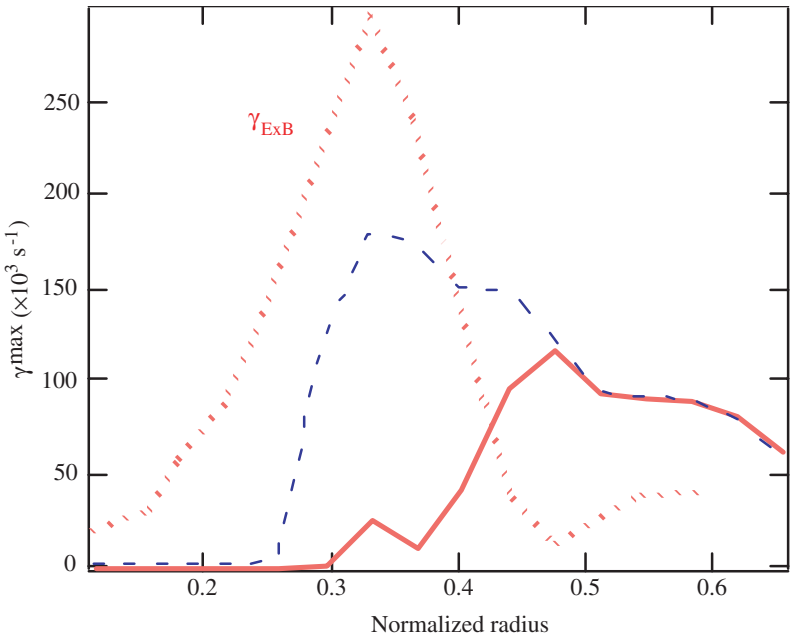

Figure 12. Comparison of $\gamma_{E\times B}$ (dot) and $\gamma^{\max}$ (for $k_\perp \rho_i < 1$) for discharge #53521 shown in figure 10, performed at the time where the ITB is fully developed ($t = 8$ s), with (——) and without α effect (- - - -).

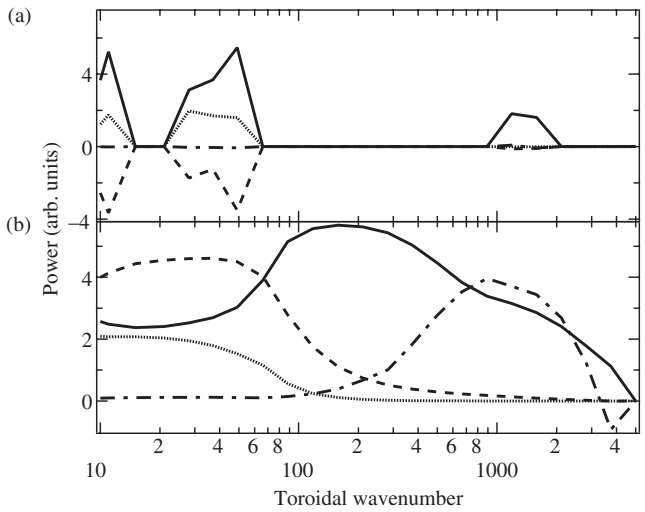

Figure 13. Mean normalized driving power of each kind of particle. ——: trapped electrons, - - - -: passing ions, dots: trapped ions, — · —: passing electrons. Same conditions as in figure 12.

the electron temperature and a decrease of the electron thermal diffusivity inside the region $r/a \leqslant 0.3$ ($q_{\min}$ is located at $r/a \approx 0.25$). Note that MHD activity analysis has identified a $m/n = \frac{3}{2}$ tearing mode as responsible for the central electron temperature roll-overs [48]. Thus, we have performed micro-stability analyses for $t = 6.4$ s (before ITB transition) and

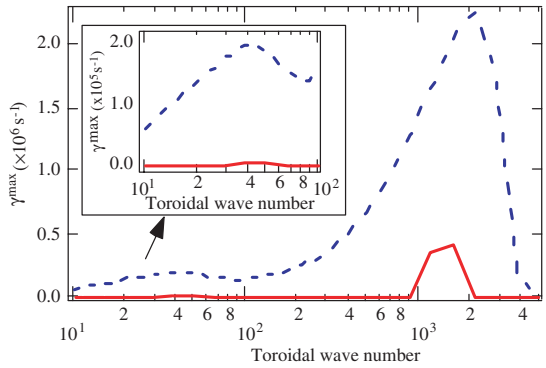

Figure 14. Spectrum of linear growth rate of discharge #53521, performed at the time where the ITB is fully developed ($t = 8$ s) for $r/a = 0.37$, compared with a computation by assuming a monotonic q-profile (- - - -).

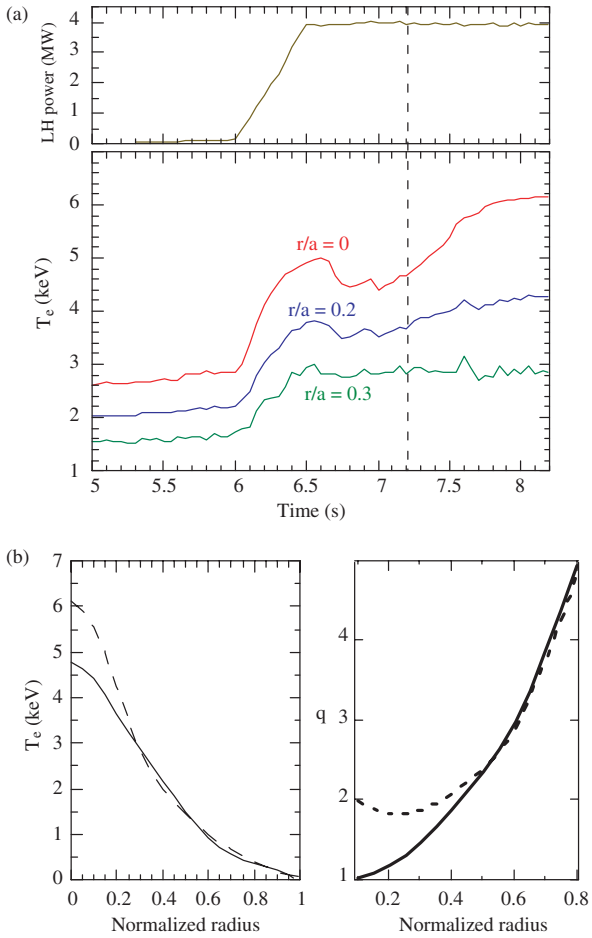

Figure 15. (*a*) Time traces of LH power and electron temperature at various radius of a Tore Supra discharge (#28334, $I_p = 0.7$ MA, $B_T = 3.9$ T and $n_e(0) = 2.5^{19}$ m^{-3}) exhibiting an electron ITB. (*b*) Electron temperature (left) and safety factor (right) profiles, at $t = 6.4$ s (——) and $t = 8$ s (- - - -).

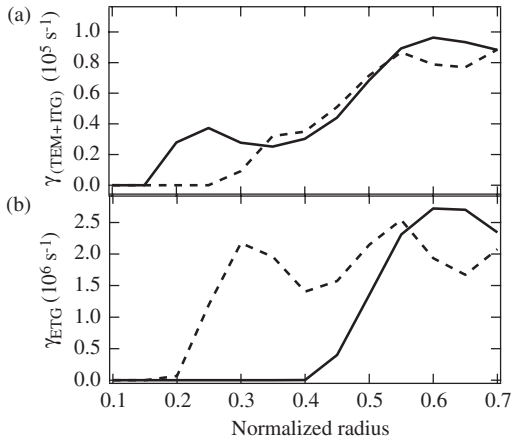

Figure 16. Linear growth rate for TEM + ITG (*a*) and ETG (*b*) modes for Tore Supra discharge #28334 described in figure 15 (——: no ITB ($t = 6.4$ s); - - - -: during ITB ($t = 8$ s)).

$t = 8$ s (during ITB). Radial profiles of $\gamma^{\max}$ for ITG + TEM and ETG modes are shown in figure 16. Evaluation of P_l shows that TEMs are mainly destabilized. Comparison of the curves obtained at 6.4 and 8 s shows that transition into the LHEP phase is characterized by

(a) Stabilization of TEMs in the plasma core, between $x = 0.1$ and $x = 0.3$. The stabilizing parameter has been identified by artificially replacing the current profile at $t = 8$ s by the current profile at $t = 6$ s. In this virtual configuration, the stabilization disappears, leading to the conclusion that in the actual case the reversed current profile is the main factor leading to stabilization of the TEMs. It is worth noting again that in this scenario with LH power only, neither $E \times B$ shearing rate nor Shafranov shift is large enough to have an effect on the stability. In addition, the effect of the density gradient has been checked and found to be insignificant.

(b) The destabilization of ETG modes between $x = 0.2$ and $x = 0.5$, due to the increase of the ETG in the LHEP phase, which overcomes the stabilizing effect of the negative magnetic shear on the ETG branch.

Thus, the transition into the LHEP phase seems to be attributable to the TEM stabilization by the reversed current profile formed by LHCD, whereas the ETG modes prevent the electron heat diffusivity to reach the neoclassical level. Note that the association of an improved electron heat transport regime with the low wavenumber mode stabilization in such a scenario is consistent with the observation of the fluctuation level in JET during the electron ITB onset in LH only heated plasmas [5].

6. Summary

In this paper, we have investigated the role of the current density profile on drift wave stability. We used the gyro-kinetic code KINEZERO that produces linear growth rate spectra with electrostatic and collisionless approximations. The individual effect of s, q and α were investigated, and a detailed analysis of the dependence of the normalized critical temperature gradient lengths on s and q was carried out. The critical thresholds are not symmetric with respect to negative/positive s values. Moreover, the thresholds of ITG-like and ETG modes are very similar for $s > 0$, whereas for $s < 0$ the ITG-like modes are more stable than the

ETG modes, resulting in higher values of $(R/L_T)_c$. This trend is due to the specific behaviour of the trapped electrons for ITG-like modes. We have proposed an empirical formula for the threshold of both positive and negative magnetic shear.

The main mechanisms responsible for the onset of ion and electron ITB in reversed shear experiments in JET and Tore Supra have been identified. In JET, ion ITBs can be triggered by the stabilization of large scale instabilities by the negative magnetic shear. The subsequent increase of the $E \times B$ shearing rate allow the ITB to expend despite the increase of the growth rates due to the temperature gradient peaking. The α stabilization is found to become important only when the ITB is fully developed. In Tore Supra LHEP modes, the electron ITB is associated with the stabilization of the large scale TEM by the negative magnetic shear effect, whereas the steep ETG destabilizes the small scale ETG modes, which prevent the electron heat transport to reach neoclassical levels.

References

[1] Taylor T S 1997 *Plasma Phys. Control. Fusion* **39** B47
[2] Gormezano C 1999 *Plasma Phys. Control. Fusion* **41** B367
[3] Hoang G T *et al* 2000 *Phys. Rev. Lett.* **84** 4593
[4] Antar G *et al* 2001 *Phys. Plasmas* **8** 186
[5] Conway G D *et al* 2002 *Plasma Phys. Control. Fusion* **44** 1167
[6] Burrel K H 1999 *Phys. Plasmas* **6** 4418
[7] Maget P *et al* 1999 *Nucl. Fusion* **39** 949
[8] Waltz R E *et al* 1994 *Phys. Plasmas* **1** 2229
[9] Dimits A M *et al* 2001 *Nucl. Fusion* **40** 1725
[10] Romanelli F and Zonca F 1993 *Phys. Fluids* B **5** 4081
[11] Garbet X *et al* 2001 *Phys. Plasmas* **8** 2793
[12] Nazikian R *et al* 1998 *Plasma Phys. Control. Nucl. Fusion Research* (Vienna: IAEA)
[13] Beer M A *et al* 1997 *Phys. Plasmas* **4** 1792
[14] Kinsey J E *et al* 2001 *Phys. Rev. Lett.* **86** 814
[15] Budny R V *et al* 2002 *Plasma Phys. Control. Fusion* **44** 1215
[16] Joffrin E *et al* 2002 *Nucl. Fusion* **42** 235
[17] Eriksson L G *et al* 2002 *Phys. Rev. Lett.* **88** 145001
[18] Litaudon X *et al* 2001 *Plasma Phys. Control. Fusion* **43** 677
[19] Hugon M *et al* 1992 *Nucl. Fusion* **32** 33
[20] Levinton F M *et al* 1995 *Phys. Rev. Lett.* **75** 4417
[21] Strait E J *et al* 1995 *Phys. Rev. Lett.* **75** 4421
[22] Ishida S *et al* 1997 *Phys. Rev. Lett.* **79** 3917
[23] Bourdelle C *et al* 2000 *Proc. 27th Eur. Conf. on Controlled Fusion and Plasma Physics (Budapest, 2000)* vol 24B, p 1092
[24] Bourdelle C *et al* 2002 *Nucl. Fusion* **42** 892
[25] Connor J W *et al* 1978 *Phys. Rev. Lett.* **40** 396
[26] Brunner S *et al* 1998 *Phys. Plasmas* **5** 3929
[27] Liu C S *et al* 1972 *Phys. Rev. Lett.* **29** 1489
[28] Hinton F L *et al* 1981 *Proc. 8th Int. Conf. on Plasma Phys. Control. Nucl. Fusion Research 1980* vol 365 (Vienna: IAEA)
[29] Horton W *et al* 1988 *Phys. Fluids* **31** 2971
[30] Romanelli F 1989 *Phys. Fluids* B **1** 1018
[31] Rebut P H *et al* 1989 *Proc. 12th International Conf. on Plasma Phys. Control. Nucl. Fusion Research 1988* vol 191 (Vienna: IAEA)
[32] Hahm T S and Tang W M 1989 *Phys. Fluids* B **1** 1185
[33] Dorland W *et al* 1995 *Proc. 15th Int. Conf. on Plasma Phys. and Control. Nucl. Fusion Research 1994* vol 463 (Vienna: IAEA)
[34] Stallard B W *et al* 1999 *Phys. Plasmas* **6** 1978
[35] Dimits A M *et al* 2000 *18th IAEA Fusion Energy Conf.* IAEA-CN-77/THP1/03
[36] Hoang G T *et al* 1998 *Nucl. Fusion* **38** 117

[37] Ryter F *et al* 2000 *18th IAEA Fusion Energy Conf.* IAEA-CN-77/EX2/2
[38] Devynck P *et al* 1997 *Plasma Phys. Control. Fusion* **39** 1355
[39] Colas L *et al* 1998 *Nucl. Fusion* **38** 903
[40] Hoang G T *et al* 2001 *Phys. Rev. Lett.* **87** 125001-1
[41] Jenko F *et al* 2001 *Phys. Plasmas* **8** 4096
[42] Litaudon X *et al* 2002 *Plasma Phys. Control. Fusion* **44** 1057
[43] Challis C D *et al* 2001 *Plasma Phys. Control. Fusion* **43** 861
[44] Waltz R E and Miller R L 1999 *Phys. Plasmas* **6** 4265
[45] Waltz R E *et al* 1997 *Phys. Plasmas* **4** 2482
[46] Hahm T S and Burrell K H 1995 *Phys. Plasmas* **2** 1648
[47] Kim Y B *et al* 1991 *Phys. Fluids* B **3** 2050
[48] Zabiego M *et al* 2001 *Plasma Phys. Control. Fusion* **43** 1625